Characterisation of silicon microstrip detectors for the ATLAS Phase-II Upgrade with a micro-focused X-ray beam

Luise Poley*[1], Andrew Blue[2], Richard Bates[2], Ingo Bloch[1], Sergio Diez[1], Javier Fernandez-Tejero[3], Celeste Fleta[3], Bruce Gallop[4], Ashley Greenall[5], Ingrid-Marja Gregor[1], Kazuhiko Hara[6], Yoichi Ikegami[7], Carlos Lacasta[8], Kristin Lohwasser[1], Dzmitry Maneuski[2], Sebastian Nagorski[9], Ian Pape[10], Peter W. Phillips[4], Dennis Sperlich[11], Kawal Sawhney[10], Urmila Soldevila[8], Miguel Ullan[3], Yoshinobu Unno[7], Matt Warren[12]

[1]*Deutsches Elektronen-Synchrotron (DESY), Notkestrasse 85, 22607 Hamburg, Germany*
[2]*SUPA School of Physics and Astronomy, University of Glasgow, Kelvin Building, Glasgow, G12 8QQ, UK*
[3]*Centro Nacional de Microelectrónica, IMB-CNM, CSIC, Barcelona, Spain*
[4]*Particle Physics Department, STFC Rutherford Appleton Laboratory, Harwell Campus Didcot, OX11 0QX, UK*
[5]*Oliver Lodge Laboratory, Department of Physics, University of Liverpool, Liverpool L69 7ZE, UK*
[6]*Institute of Pure and Applied Sciences, University of Tsukuba, Tsukuba, Ibaraki 305-8751, Japan*
[7]*Institute of Particle and Nuclear Study, KEK, Oho 1-1, Tsukuba, Ibaraki 305-0801, Japan*
[8]*Universidad de Valencia - Instituto de Física Corpuscular (IFIC) Edificio Institutos de Investigación, c/ Catedrático José Beltrán, 2, E-46980 Paterna, Spain*
[9]*School of Physics, Dublin Institute of Technology, Kevin Street, Dublin 2, Ireland*
[10]*Diamond Light Source Ltd, Diamond House, Harwell Science and Innovation Campus, Didcot, Oxfordshire, OX11 0DE, UK*
[11] *Humboldt-Universität zu Berlin, Newtonstraße 15, 12489 Berlin, Germany*
[12]*Department of Physics and Astronomy, University College London, Gower Street, London, WC1E 6BT, UK*

E-mail: Anne-Luise.Poley@desy.de

The planned HL-LHC (High Luminosity LHC) in 2025 is being designed to maximise the physics potential through a sizable increase in the luminosity, totalling $1x10^{35}cm^{-2}s^{-1}$ after 10 years of operation. A consequence of this increased luminosity is the expected radiation damage at $3000fb^{-1}$, requiring the tracking detectors to withstand hadron equivalences to over $1x10^{16}$ 1 MeV neutrons per cm^2. With the addition of increased readout rates, a complete re-design of the current ATLAS Inner Detector (ID) is being developed as the Inner Tracker (ITk).

Two proposed detectors for the ATLAS strip tracker region of the ITk were characterized at the Diamond Light Source with a 3µm FWHM 15keV micro focused X-ray beam. The devices under test were a 320µm thick silicon stereo (Barrel) ATLAS12 strip mini sensor wire bonded to a 130nm CMOS binary readout chip (ABC130) and a 320 µm thick full size radial (Endcap)

strip sensor - utilizing bi-metal readout layers - wire bonded to 250nm CMOS binary readout chips (ABCN-25).

Sub-strip resolution of the 74.5µm strips was achieved for both detectors. Investigation of the p-stop diffusion layers between strips is shown in detail for the wire bond pad regions. Inter strip charge collection measurements indicate that the effective width of the strip on the silicon sensors is determined by p-stops regions between the strips rather than the strip pitch. The collected signal allowed for the identification of operating thresholds for both devices, making it possible to compare signal response between different versions of silicon strip detector modules.

KEYWORDS: Instrumentation for particle accelerators; Hybrid detectors; Inspection with X-rays; Si microstrip and pad detector

* Corresponding author.

Contents

1. Introduction

Around 2025, the Large Hadron Collider (LHC) at CERN will be upgraded to an instantaneous luminosity of $L=10^{35}cm^{-2}s^{-1}$ from previously $L=10^{34}cm^{-2}s^{-1}$ (High Luminosity LHC) [1]. The simultaneous upgrade of the ATLAS detector at the LHC will require the replacement of the current ID with a new Inner Tracker (ITk) [2].

Unlike the current Inner Detector (ID), the ITk will be an all-silicon tracker, constructed to maintain tracking performance in the high occupancy environment and to cope with the increase of approximately a factor of ten in the total radiation fluence. New technologies are used to ensure that the system can survive this harsh radiation environment and to optimise the material distribution, while the new readout scheme allows the implementation of a track trigger contributing to the improvements in the ATLAS data taking capabilities.

The ITk will consist of both pixel and strip detectors, consisting of a central barrel region between +/-1.3m and two end-caps that extend the length of the strip detector to +/-3m. The detectors cover +/- 2.5 units of rapidity [2].

Silicon strip sensors for the future ATLAS detector have been developed, and detector module prototypes have been constructed [3]. In ongoing R&D efforts, current versions of module components are improved towards designs suitable for the future ATLAS strip tracker. The performance of new components in detector modules can be analysed by comparing the signals collected for a given range of thresholds set for the binary readout chip.

This paper describes the use of a micro focused X-ray beam for fine strip scans across several sensor strips [4,5]. The scan was conducted to compare the signals collected for two silicon strip detector modules from two successive module designs in order to investigate the performance of a new binary readout chip (ABC130) compared to its previous version (ABCN-25), as well as the new ATLAS12 strip layout.

2. Devices

The devices investigated in the testbeam were constructed as similarly as possible to future strip tracker modules with the components currently available [6]. Each module consisted of a prototype of an actual silicon micro strip sensor, on to which a hybrid with front-end readout chips was glued [7]. Aluminium wedge wire bonding was used both to connect the sensor strips and ASIC readout channels and to connect the ASICs and hybrid electrically. Both devices are described in detail in the following sections 2.1 & 2.2. The devices were mounted on test frames, which provided high voltage to bias the sensor as well as low voltage to power the hybrid and an interface to the readout electronics.

The strip sensors used in both modules were AC-coupled with n-type implants in a p-type float-zone silicon bulk (n-in-p FZ). This type of sensor collects electrons and has no radiation induced type inversion. Signals were read out using an FPGA Development board (ATLYS) with the C++ based framework SCTDAQ, which was developed for the Semiconductor Tracker (SCT) in the current ATLAS detector and modified for the operation of modules for the future ATLAS strip tracker.

In preparation of being operated in the test beam, both devices were tested in the lab using the SCTDAQ framework. The performance of all readout channels (input noise and gain) was determined using known injected charges, generated on calibration capacitors present on the ASIC. All channels were trimmed to a charge of 0fC for a defined threshold.

2.1 ABCN-25 Endcap Module

The module built using ABCN-25 binary readout chips was an end-cap module constructed at DESY. It consisted of a hybrid with 12 ABCN-25 readout chips [8] that had been glued on to two silicon sensors (see Figure 1). The sensors were designed and fabricated at CNM-Barcelona. They had a thickness of 320µm and a length of 38.7µm with two rows of sensor strips. The circular shape of the end-cap leads adjacent sensor strips having pitches increasing towards outer radii from 67µm to 106µm [9].

This module was constructed as part of a study to investigate alternative sensor layouts, which used a second metal layer to modify the sensor bond pad layout for a faster and more reliable wire bonding process compared to the baseline layout [10], and alternative to the standard pitch adapters [11]. However, the presented fine strip scan was conducted in a sensor area without a second metal layer in order to eliminate influences by layout changes.

The module was operated at a reverse bias voltage of 120V (over-depleted, $V_{FD} \approx 47$ V). The device was operated on an aluminium plated jig cooled down to 10°C by a chiller to compensate for the heat produced by the readout chips (~300mW per ABCN-25 ASIC)[8].

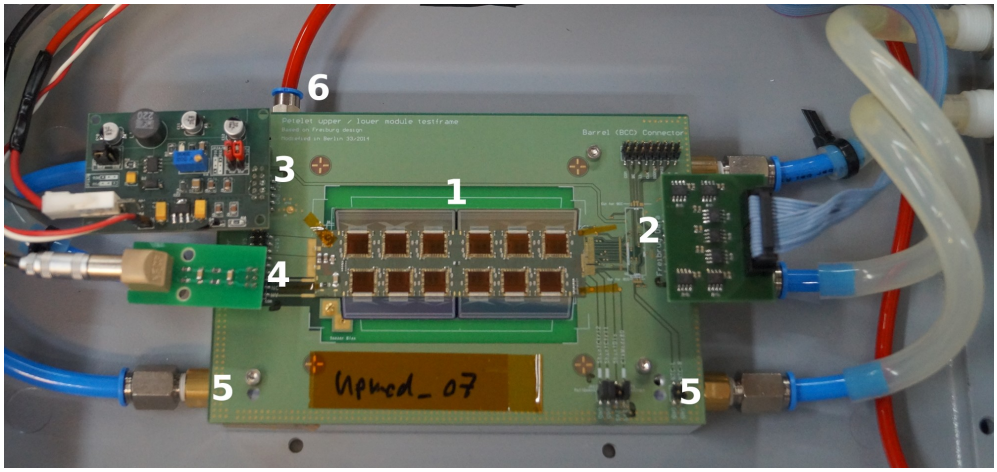

Fig 1: ABCN-25 end-cap module as operated in the test beam. The module (1) was mounted on a test frame with a connector for data readout (2), low voltage (3) to power the module, high voltage (4) to bias the sensor, cooling tubes (5) leading through the mounting jig and a vacuum line (6) for a good contact between module and cooling jig.

2.2 ABC130 Mini Module

The baseline design of the new strips tracker envisages binary readout by means of the ABC130 readout ASIC [7,12], fabricated in the 8RF 130nm CMOS technology from IBM Semiconductors. The first batch of ABC130 was produced and delivered in November 2013 and is currently under test. The current proposal is that any future CMOS ASIC for the ITK Strips will utilise the same front-end designs.

Preliminary tests of the initial production of the ABC130 chips have been performed. Communication and configuration of the chips work correctly. Data passing at a readout rate of 80MHz has been performed, and the current consumption of the chip has been vastly reduced (as expected as a consequence of the 130nm process) to give an estimated 3W/module, as compared to the current 20W/Module for the present ABCN-25 chip fabricated in the 250nm process.

To further test the new ABC130 readout chip and ATLAS12 strip layout a mini version of a full-scale module was assembled at Liverpool and RAL. Three ABC130 chips were glued to a FR4 hybrid, with two of these wire bonded to ATLAS12 mini sensors [13]. The mini sensors under test consisted of 256 strips (74.5um pitch in 2 rows) utilising punch through protection (PTP) structures with an overall size of 1x1cm^2.

All data was multiplexed through the hybrid control chip (HCC), and routed via a custom designed PCB along with HV and LV connections. The HCC interfaces the ABC130 ASICs on the hybrid to the to end of structure electronics.

A reverse bias of 300V was applied to fully deplete the mini sensors. The low power output meant that the detector did not have to be cooled whilst in operation.

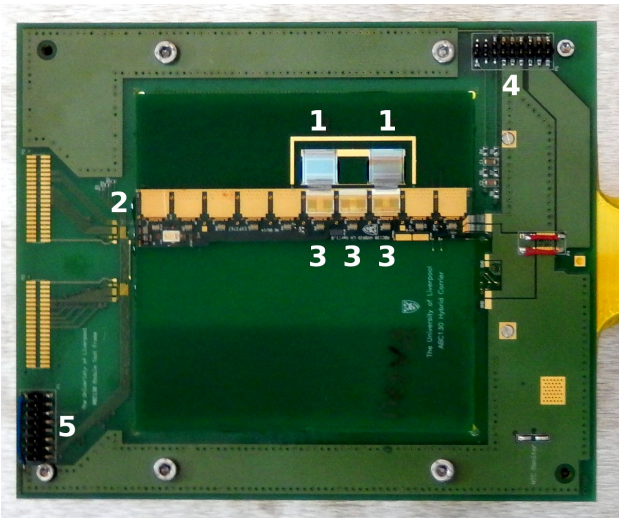

Fig 2: Device mounted on test frame. The device consists of two miniature prototypes of ATLAS silicon strip sensors (1), a hybrid (2) with three ABC130 readout chips (3), wire bonded to the miniature sensors. The device is mounted on a test frame, which provides power (4) and provides an interface to the readout electronics (5)

3. Synchrotron Technique

To study the inter-strip resolution of the detectors, we desire both a high rate of signal with a monochromatic energy and a beam spot to be smaller in size than the silicon detector strip pitch

(74.5 µm). Due to both sets of readout chips operating in binary readout mode, we would also like the interactions to occur with minimal X- ray photons per acquisition.

For these reasons, we cannot use radioactive source measurements for these tests, laser tests or conventional particle testbeams. TCT (Transient Current Technique) measurements are a viable candidate but measurements cannot be made below any metal surfaces of the detector. However, such measurements can be performed using a micro focused monochromatic X-ray beam. With the additional ability to accurately control the position of the beam, it makes it ideal to perform such studies at a synchrotron.

3.1 X- Ray Beam

The measurements presented here were all performed at the B16 beamline at the Diamond Synchrotron Light Source. This beam line comprises of a water-cooled fixed-exit double crystal monochromator that is capable of providing monochromatic beams over a 4-20keV photon energy range. An unfocused monochromatic beam is provided to the experimental hutch. A compound refractive lens (CRL) was used to produce a 15keV micro-focused X-ray beam.

The size of the micro-focused beam was determined by measuring transmissions scans with a 200µm gold wire. Scans were made in both x and y across the beam, and the derivative of these scans indicated the beam size to have a σ = 3.3µm & 1.7µm in the horizontal and vertical directions respectively (Figure 3).

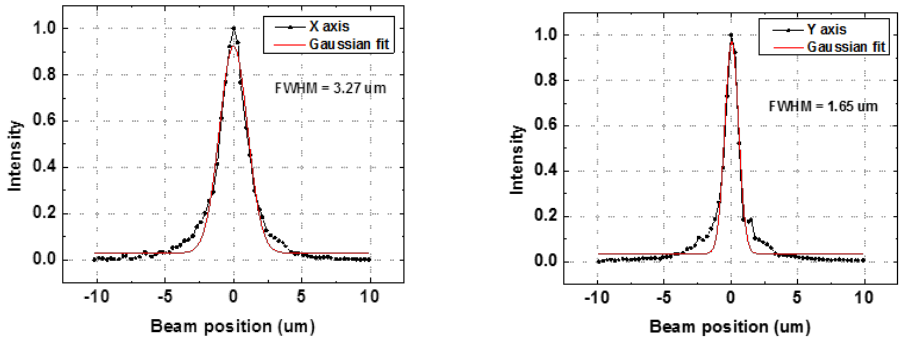

Figure 3: Diamond X-ray beam profiles measured using a gold wire. (a) Beam width in x was measured 3.27µm (b) Beam width in y was measured 1.65µm

3.2 DAQ & Readout

For data acquisition, a machine trigger from the beam was reduced from 2MHz to 1 kHz and fed in to the Digilent ATLYS readout board utilising a Xilinx Spartan 6 LX45 FPGA. ATLYS is a low-cost, widely available board that has sufficient resources to support single chip, hybrid

and module tests. The board had the Adept programming interface allowing it to be programmed with a USB cable. This made it easy to reprogram and consequently it was possible to test 2 modules with different firmware versions with only 1 development board.

Control of the device under test (DUT) stage (X, Y and Z) was done using custom Python scripts. A signal was sent after the stage movement was complete to the DAQ to start the data acquisition. This allowed for a highly automated, fast and efficient run control for all scans taken during the allocated beam time.

With both detectors operating a 40MHz clock, it was expected based on the beam current that there was average of 2-3 photons traversing the silicon sensors in the 25ns collection time. Since each 15keV photon has 51.07% chance of interaction with 320µm silicon [14], the vast majority of acquisitions contained single X-ray photon events, with each 15keV interaction depositing ~4.2k electrons (due to the 3.6eV electron hole pair creation energy of Silicon). This is equivalent to 0.673fC, corresponding to a threshold of 80-90 mV in the investigated devices. All data was written to disk by the DAQ as custom histograms, and analysis scripts written in to study signal response and at various positions and thresholds.

3.3 Device Mounting and Alignment

Both detectors were mounted in custom designed Aluminum test boxes that had connections for voltage, data, grounding and cooling (for the 250nm endcap module). In each case the DUTs were mounted so that the X-ray beam was perpendicular to the sensor surface. The test box was then mechanically mounted to a set of stages, allowing for fine movement control in X (across strips), Y (along strips), and Z (along beamline) (Fig 4).

Both boxes used kapton tape the front and back to shield the silicon from visible light effects but have minimal X-ray attenuation. A scaled CAD drawing of the module was attached to the font of each box, allowing for first alignment of the beam on the sensitive silicon area.

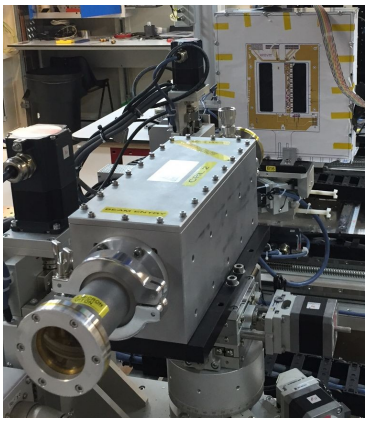

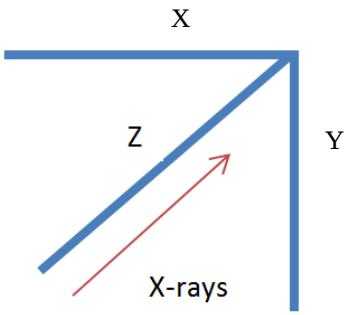

Figure 4: (Left) The Barrel Mini Module test box attached to the XYZ stage in the beam; (Right) a schematic of the DUT stage orientation

4. Results

The X-ray beam diameter of 3.3 x 1.7μm was sufficiently small compared to the strip pitch to resolve the transverse sensor structure by performing threshold scans at each different beam position across the strips. Threshold scans across three sensor strips were performed for both devices in either 5 or 10μm steps recording the hit occupancy. Table 1 shows an overview of the scanning parameters for both devices.

	End-cap Module	**Barrel Mini Module**
Strip pitch [μm]	*103*	*74.5*
p-stop type	*regular*	*irregular*
Scan length [μm]	*190*	*210*
Position step size [μm]	*10*	*5*
Threshold range [mV]	*150-515*	*205.1-530.1*
Trimming	*0 fC = 70mV*	*0 fC = 132.1mV*
Triggers per threshold	*3500*	*10000*
Readout chips	*ABCN-25*	*ABC130*

Table 1: Overview of the scanning parameters performed for two silicon strip sensors

With these scans, the influence of p-stop regions on the overall signal shape was also investigated. P-stops are implanted in the p-doped sensor between the n-doped strips in order to avoid short-circuits on the sensor surface after irradiation. On most of the sensor area, p-stops are implanted parallel to the strips with equal distances to both adjacent strips, but where the strips are connected to the readout channels of a front-end-chip via wire bonds, p-stops are placed around the required aluminium bond pads (see Figure 5).

Positioning p-stops at a sufficient distance from the wire bond pads leads to uneven distances to the adjacent sensor strips on the left and right side of the p-stop. In the ATLAS12 mini-sensors under test, the wire bond pad structures account for 1/3 of the sensor surface.

The effects of these p-stop shapes were investigated by scanning across one of this region of the sensor and are shown in section 4.2. Comparative scans were also made in the centre of the conventional p stop doping regions.

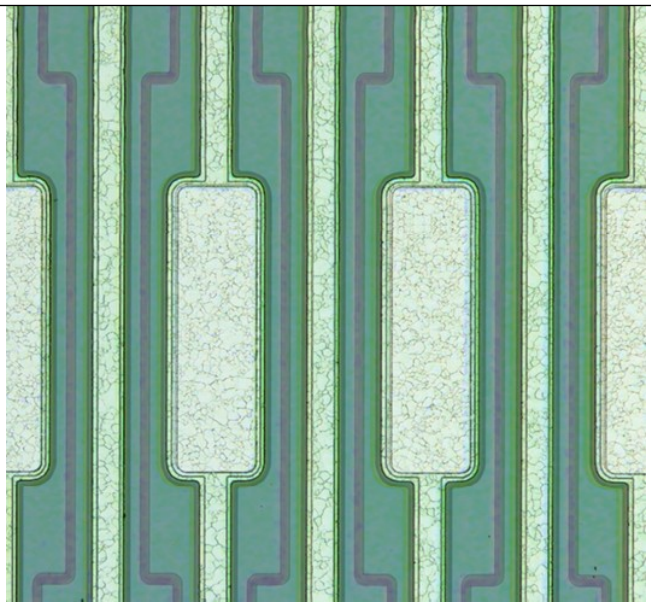

Figure 5: Silicon strip sensor with a strip pitch of 74.5 µm. Aluminium bond pads are added to the strips for electrical connections between sensor strips and readout channels by wire bonds. With the width of the bond pads being close to the strip pitch, the p-stops need to be guided around the bond pads, leading to a larger distance to the sensor strip beneath the bond pad and a smaller distance to the adjacent strip without a bond pad. The alternating distances between p-stops and strips lead to alternating p-stop widths around a strip.

4.1 ABCN-25 Module

Figure 6 shows the results for threshold scans - a scan varying the minimum integrated charge over which the binary readout registers a hit - across three strips (10µm steps) of an end-cap sensor. The signals obtained from an individual channel show the expected behaviour: over a scan distance of 100 µm, matching the sensor strip pitch in that region of 103µm, the channel shows signals up to high thresholds. Outside the region of the central strip, high signal levels were measured for low thresholds, corresponding to noise. In the transition between both regions, the registered number of signals is smaller than in the main sensor region.

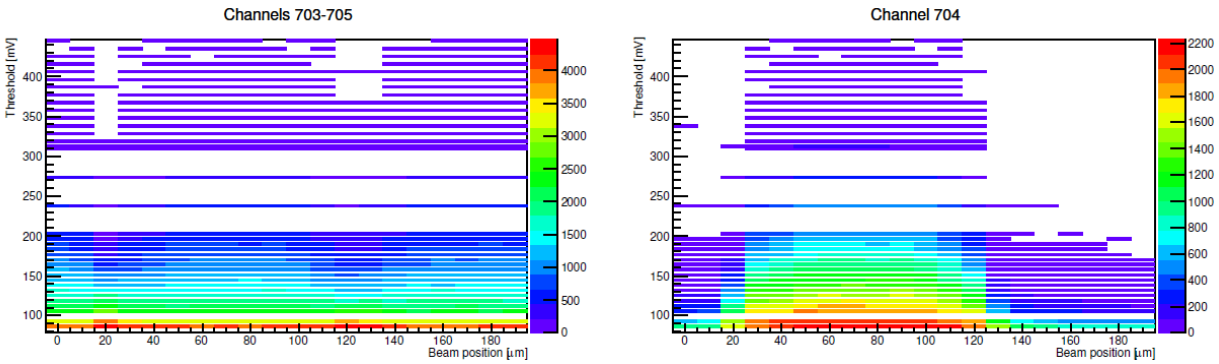

Figure 6: Number of registered signals over threshold as a function of threshold at a beam position for either three adjacent channels (left) and the central channel only (right)

The signals from three adjacent strips, measured at the nominal threshold of 105.6mV, are shown in Figure 7. All three strips under investigation show the same signal height and shape across the strip, with the width of the signals matching the strip pitch of the sensor.

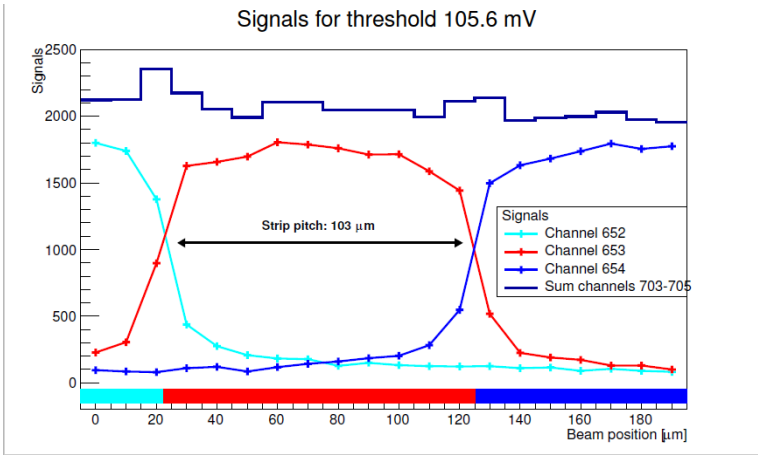

Figure 7: Combined signals from three adjacent strips for a fine strip scan across three strips, showing the individual signals at a 105.6 mV. The collected signals for the channels fit the positions of the strips as well as the sensor strip pitch well.

The integrated signals show different shapes depending on the threshold (see Figure 8). For low thresholds, transition regions between adjacent channels exhibit higher signal numbers due to charge sharing between these channels, so consequently hits were registered twice. Conversely high thresholds at the same transition regions, register less hits in adjacent strips. As a consequence, low thresholds show a signal level above average over strip borders and high thresholds show a lower signal levels in the same region.

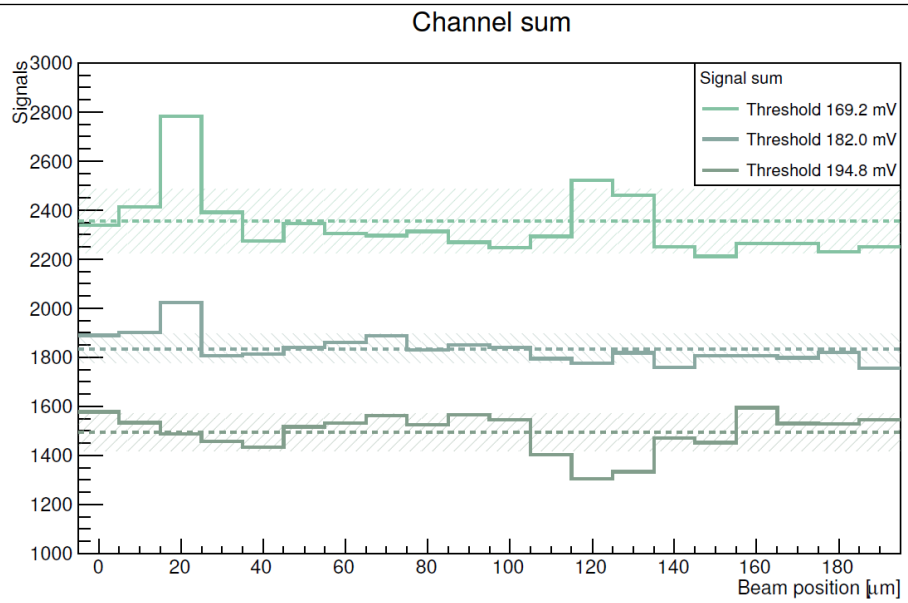

Figure 8: Integrated signals for three adjacent channels at different thresholds, with the average and 1 sigma deviation shown for each threshold. For a threshold of 182.0 mV, the integrated signals for all beam positions show a distribution with a smaller deviation than higher and lower thresholds

Figure 9 shows different signal ratios compared to find a good working point. The ratios of minimum signal sum to both average and maximum signal sum were found to be at a maximum for this threshold, indicating a small variation of the collected signal sum, which matches the small overall standard deviation. At a threshold of 182.0 mV, the relative average signal sum was below 1, i.e. not dominated by noise, but close to 1, indicating a high efficiency.

These scans allowed for the comparison of the integrated signals for all thresholds at different beam positions. The optimal operating point was chosen such that the integrated signals were constant for all beam positions, i.e. to show neither charge loss nor double counted signals over the p-stop regions.

The fine strip scan performed on an end-cap sensor confirmed the expected signal levels and shapes both for an individual channel and the integrated signals of three adjacent channels. Furthermore, the collected integrated signal allowed to find a good operating threshold for the expected size of signal for this device by comparing the signals collected at different thresholds.

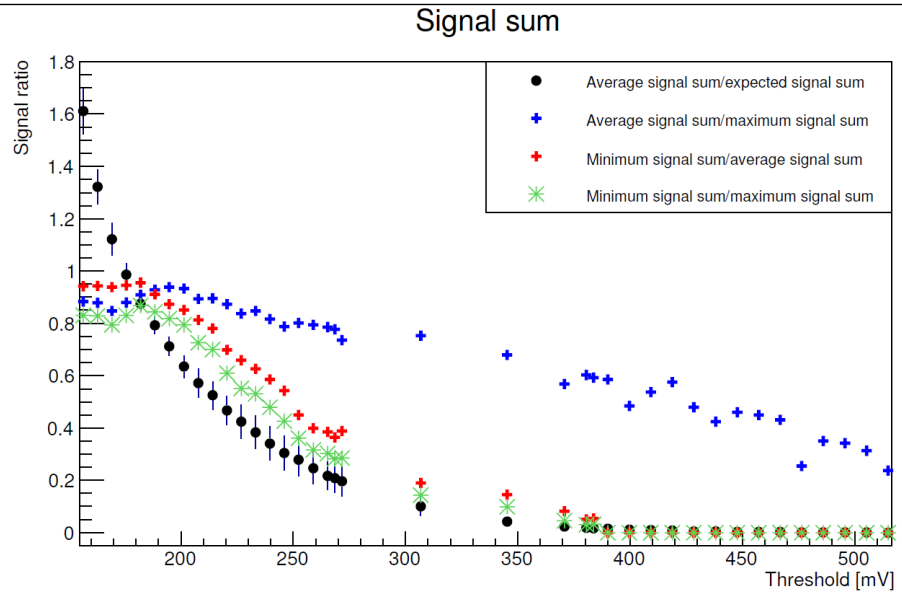

Figure 9: Comparison of collected signal sums for all thresholds used in the scan for the selection of a working point. The figure shows the average sum of collected signals in three adjacent strips relative to the number of expected signals (black), as well as the ratios of minimum, maximum and average signal sums of all beam positions.

4.2 ABC130 Mini Module

The results from scanning across three strips in 5µm steps are shown in Figure 10. The scan shows different widths of signal detection ranges for adjacent strips: alternating channels show an alternating succession of larger and smaller detection areas.

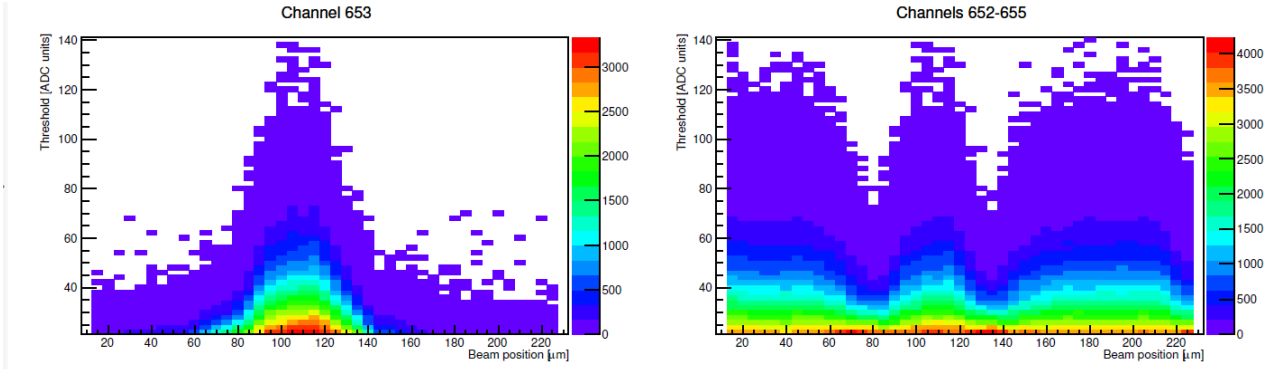

Figure 10: Fine strip scan across three strips of a mini sensor connected to a barrel hybrid for only the central strip (left) and three adjacent strips (right), measured for different beam positions and thresholds

Independent of the width of the detection range, the number of detected signals at the central region of a channel is similar for all channels. Comparing the width of the channels' detection ranges to the sensor geometry, the detected signals were found to agree well with the p-stop geometry in the measured area (see Figure 11).

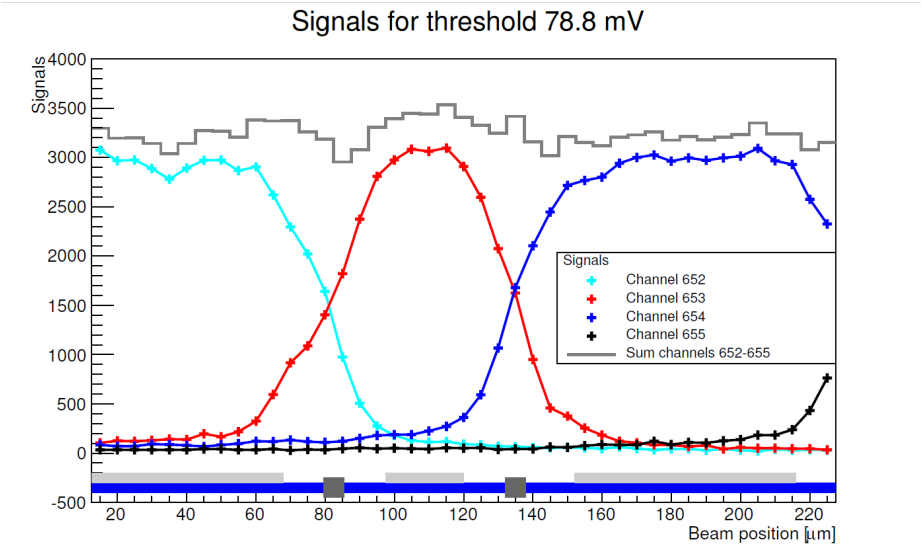

Figure 11: Signals from four adjacent channels and their sum at a possible operating threshold of 80mV with the corresponding sensor geometry: silicon (blue), aluminium layer (light grey) and p-stops (dark grey). The signals can be seen to agree well with the measured geometry

Figure 12 shows an overview of the integrated signal for four adjacent channels for four different thresholds. Similar to the results for the end-cap sensor, the collected signals were found to either show maxima over p-stops between strips for low thresholds or minima for high thresholds due to charge sharing.

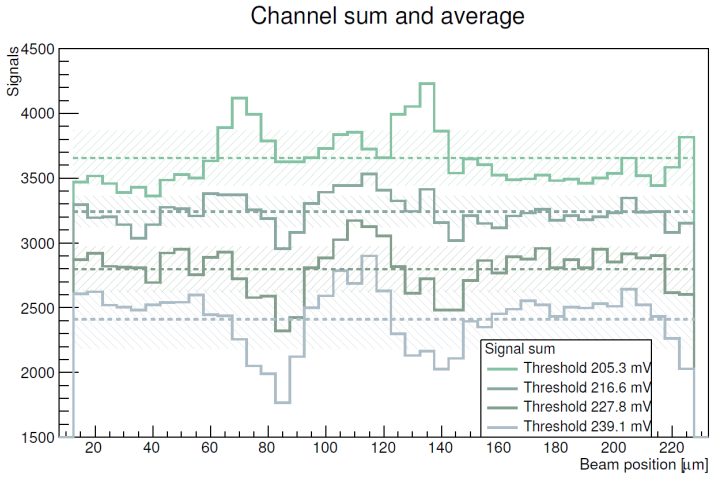

Figure 12: Integrated signal for four adjacent channels for different beam positions and thresholds, shown with the average collected signal sum and 1 sigma deviation shown for each threshold. For a threshold of 216.6 mV, the collected signal sum across three strips was found to be flatter than for higher or lower thresholds.

The signal sum shapes for different thresholds were compared in order to find a good working point, i.e. a signal sum across several sensor strips (Figure 13). Similar to the analysis of the end-cap sensor scan results, a good working point was selected by choosing a high efficiency with a small standard deviation as well as a high ratio between minimum average and maximum signal sum.

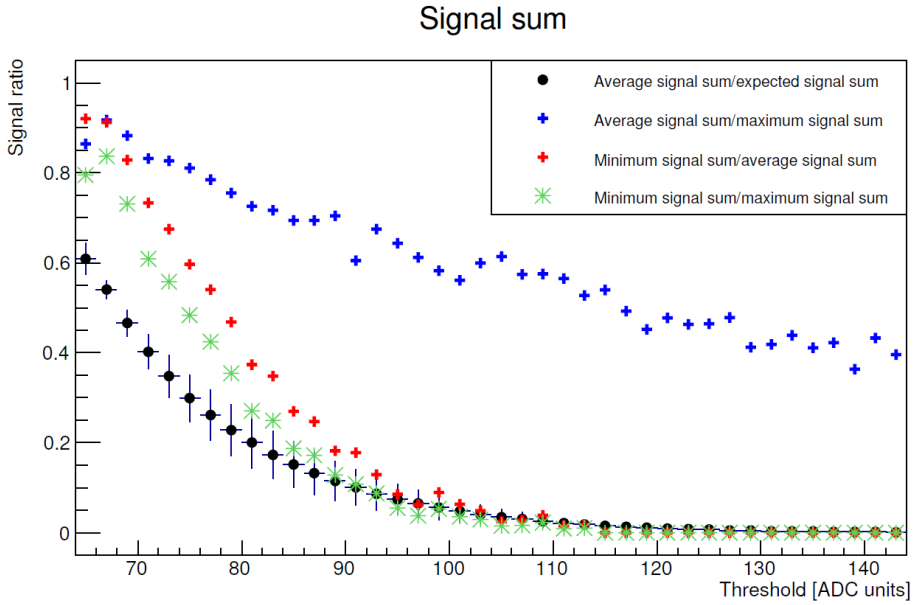

Figure 13: Comparison of collected signal sums for all thresholds used in the scan for the selection of a working point. The figure shows the average sum of collected signals in three adjacent strips relative to the number of expected signals (black), as well as the ratios of minimum, maximum and average signal sums of all beam positions.

Using the scan results, a threshold of 67 ADC counts = 211.0mV was found to be a good working point for this device. It should be noted that this working point, determined by comparing signal flatness for different thresholds, provides a signal efficiency for a 15KeV X-ray to be ~54%, compared to an efficiency of ~87% for the end-cap sensor

4.3 Comparison

The analysis of the signals collected in two fine strip scan provided a direct comparison between both devices (see Figure 14). The numbers of collected signals with respect to the expected number of signals were found to be comparable in the threshold region investigated for both devices. Analysing the signal flatness across the scan shows a higher good working point

threshold for the barrel module than for the end-cap module, translating to a lower number of collected signals for the barrel hybrid the determined working point.

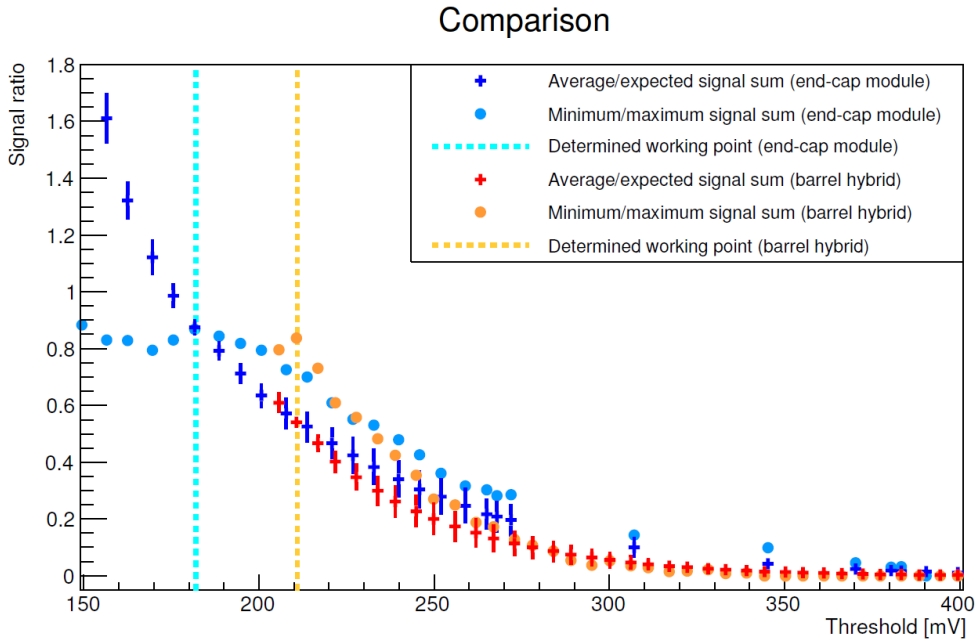

Figure 14: Comparison of the collected signal and its shape across several strips for an end-cap module and a barrel hybrid over the threshold range under investigation of up to 400 mV

The lower efficiency for the barrel module could be related to the decrease in sensor strip pitch compared to the endcap module. Previous work with analogue readout systems indicated a maximum of ~90% signal collection with an identical strip pitch [4].

5. Conclusions & Future Work

X-ray beam scans in steps of 5µm and 10µm were performed for two silicon strip detector modules for the ATLAS Phase-II Upgrade. The results show that the effective width of silicon strip sensors is determined by p-stops between the strips rather than the strip pitch. The collected signals allowed the identification of a threshold that provided a good working point for both devices and to compare different versions of silicon strip detector modules (see Table 2).

	End-cap module	**Barrel hybrid**
Threshold [mV]	*182.0*	*211.0*
Signal efficiency [%]	*87.5 +/- 2.8*	*54.0 +/- 2.0*
Signal minimum/average [%]	*95.6*	*91.2*
Signal minimum/maximum [%]	*86.8*	*83.6*
Signal average/maximum [%]	*90.8*	*91.7*

Table 2: Working points and corresponding signal properties for two devices determined from fine strip scans

Future plans for the investigations of silicon strip modules foresee a crosscheck of the results found using an X-ray beam by using an electron particle beam. Additionally, the measurements performed for non-irradiated sensors are planned to be repeated using hadron irradiated silicon

sensors in order to analyse changes in signal collection and efficiency caused by radiation damage.

6. Acknowledgments

We thank Diamond Light Source for access to beamline B16 (proposal number MT11639) that contributed to the results presented here. The authors would like to thank personnel of the B16 beam, especially Andy Malandain and Julien Marchal for providing advice, support and maintenance during the experiment.

References

[1] L Rossi., *LHC Upgrade Plans: Options and Strategy*. (CERN-ATS-2011- 257):6 p, Dec 2011.

[2] Collaboration ATLAS. *Letter of Intent for the Phase-II Upgrade of the ATLAS Experiment. Technical report*, CERN, Geneva, Dec 2012.

[3] P.P. Allport, et al., *Progress with the single-sided module prototypes for the ATLAS tracker upgrade stave*, Nuclear Instruments and Methods in Physics Research Section A: Accelerators, Spectrometers, Detectors and Associated Equipment, 636(1, Supplement):S90-S96, 2011. 7th International Hiroshima Symposium on the Development and Application of Semiconductor Tracking Detectors.

[4] D. Maneuski, R. Bates, A. Blue, C. Buttar, K. Doonan, L. Eklund, E.N. Gimenez, D. Hynds, S. Kachkanov, J. Kalliopuska, T. McMullen, V. O'Shea, N. Tartoni, R. Plackett, S. Vahanen, and K. Wraight., *Edge pixel response studies of edgeless silicon sensor technology for pixelated imaging detectors*, Journal of Instrumentation, 10(03), 2015.

[5] A. Blue et al., *Characterisation of edgeless technologies for pixelated and strip silicon detectors with a micro-focused X-ray beam' Journal of Instrumentation*, Volume 8, 2013.

[6] ATLAS ITK Strip petalet collaboration, *Development and investigation of hybrids and modules for the phase-ii upgrade of the forward region of the silicon strip tracking detector of the atlas experiment*. (in preparation to be submitted to Nucl. Instrum. Meth. A (2015).

[7] K Mahboubi, A Greenall, P P Allport, A A A_older, MWormald, A Smith, J Carroll, S Wonsak, C L Llacer, J Bernabeu, R Marco-Hernandez, C Garcia, D S Munoz, I M Gregor, M Stanitzki, D Ariza, I Bloch, C Friedric, L Poley, L Rehnisch, R Mori, M M Hauser, S Kuehn, K Jakobs, and U Parzefall. '*The front-end hybrid for the ATLAS HL-LHC silicon strip tracker*. Journal of Instrumentation' 9(02), 2014.

[8] W. Dabrowski, et al. "Design and Performance of the ABCN-25 readout chip for the ATLAS inner detector upgrade" IEEE Nuclear Science Symposium Conference Record, NSS/MIC 2009, Orlando, USA, 2009.

[9] Victor Hugo Benitez Casma et al. *Sensors for the End-Cap Prototype of the Inner Tracker in the ATLAS Detector Upgrade. Technical Report* ATL-COM-UPGRADE-2015-027, CERN, Geneva, Sep 2015.

[10] Miguel Ullan, Victor Benitez, Giulio Pellegrini, Celeste Fleta, Manuel Lozano, Carlos Lacasta, Urmila Soldevila, and Carmen Garcia., *Embedded pitch adapters for the ATLAS tracker upgrade*, Nuclear Instruments and Methods in Physics Research Section A: Accelerators, Spectrometers, Detectors and Associated Equipment, 732:178-181, 2013.

[11] M. Ullan, M. Lozano, F. Campabadal, C. Fleta, C. Garcia, F. Gonzalez, and J. Bernabeu.., *High-pitch metal-on-glass technology for pad pitch adaptation between detectors and readout electronic*s, Nuclear Science, IEEE Transactions on, 51(3):968-974, June 2004.

[12] J. Kaplon and M. Noy. “Front end electronics for SLHC semiconductor trackers in CMOS 90 nm and 130 nm processes”, IEEE Trans. on Nuclear Science, vol. 59, Issue 4, pag. 1611, 2012.

[13] Y. Unno et al., *Development of n+-in-p large-area silicon microstrip sensors for very high radiation environments – ATLAS12 design and initial results,* Nucl.Instrum.Meth. A765 (2014) 80-90, 2014.

[14] P.J. Linstrom and W.G. Mallard, Eds**.,** *NIST Chemistry WebBook, NIST Standard Reference Database Number 69***,** **N**ational Institute of Standards and Technology, Gaithersburg MD, 20899, http://webbook.nist.gov, (retrieved December 11, 2015).